Geodetic observations of the M 5.1 January 29, 1994 Northridge aftershock

Andrea Donnellan and Frank H. Webb
Jet Propulsion laboratory, Pasadena, California

Short title: GEODETIC OBSERVATIONS OF A M 5.1 NORTHRIDG E AFTERSHOCK

Abstract. Geodetic observations of the January 29, 1994 M 5.1 aftershock to the Northridge earthquake are consistent with seismic solutions showing left-lateral oblique slip on a northeast-southwest striking steeply dipping fault. Thirty second solutions of the data from the station showing the maximum observed displacement (35 mm) indicate no precursor and no immediate post-seismic motion to the aftershock. The aftershock does appear to be superimposed over the longer term Northridge post-seismic deformation field. Inversions of the data yield a potency of $2.6 \pm 0.3 \times 10^{-3} km^3$ implying a rigidity of $1.9 \pm 0.2 \times 10^{11} dyne/cm^2$. The geodetically determined rigidity is consistent, with rigidity determined from P and S wave velocities of the area.

Introduction

The M_w 6.7 Northridge earthquake occurred on January 17, 1994 at 4:31 am in the densely populated San Fernando Valley [*Jones et al.*, 1994]. The earthquake ruptured a south-dipping thrust fault from a depth of 18 km northward into the Santa Susana Mountains to a depth of 5 km. Several large aftershocks occurred in the two days following the earthquake and the aftershock sequence decayed in a normal manner with time [*Hauksson et al.*, 1995]. Two M >5 aftershocks occurred later in the sequence, a M 5.1 on January 29, 1994 in the Santa Susana Mountains, and a M 5.2 on 11 March 20, 1994 under the San Fernando Valley.

The first aftershock (January 29, 1994) was very shallow bad on first motion mechanisms, occurring at a depth of 1.59 km [*Hauksson et al.*, 1995]. The mechanism shows primarily left lateral motion with a small normal component, to it on a nearly vertical north-clipping fault (Table 1). The plane strikes northeast-southwest and was located at the northwest corner of the Northridge rupture zone and aftershock sequence. The second aftershock showed oblique left-lateral thrusting on a south-dipping fault 14.6s km deep.

Table 1

GPS data were being collected at stations near the epicenters of both of these aftershocks when they occurred (Figure 1). We see significant offsets in the GPS data for the shallow first aftershock (January 29) and no detectable motion from the deeper second aftershock (March 20). Results from the GPS data enable us to put constraints on the mechanism of the January 29 aftershock and also place bounds on the crustal rigidity in the region of the event.

Figure 1

Geodetic Observations

We analyzed the GPS data using GIPSY/OASIS II [*Zumberge et al.*, 1997] in 24 hour solutions. Since we saw no detectable motion for the March 20 aftershock we did not pursue further analysis of those data. For the January 29 aftershock we analyzed

the data in approximate 12 hour solutions before and after the earthquake for the day of the earthquake and also in 30 second solutions for the station SAFE. We fixed ambiguities and transformed the data such that far-field fiducial stations (Goldstone, Harvest, Quincy, and Vandenberg) snowed no offset or scatter during the time period.

The time series of the data show offsets near the epicenter of the aftershock and little motion in the far field (Figure 2). Both LNCH and SAFE show a drift through the time series that is most likely attributable to post-seismic motion from the Northridge mainshock. CSUN and I, NC II, located southeast of the event, show offsets to the cast and JPL shows a large offset to the south and a smaller offset to the west. It appears that at station SAFE the post-seismic and coseismic motions result from the same stress field. JPLM located nearly 50 km from the aftershock shows negligible motion during the entire time period and also the clay of the event. To calculate the station offsets (Table 2) we opted to use data from just the day of the event in order to minimize error from both daily scatter and pc)st-seismic transient motions.

Figure 2

Table 2

The north offset of SAFE is large enough to show up in 30 second kinematic solutions. We calculated 30 second solutions for this station on the clay of the aftershock to look for either pre- nor post-seismic motions. Although the scatter in these solutions is about 1 cm it is clear that the data show only a step at the time of the earthquake (Figure 3). Neither pre- or post-seismic motions are observable. Over a longer time period it appears as if a pre-seismic signal on the order of about 7 mm may have occurred, but the signal is only marginal at best.

Figure 3

Inversions

We inverted the data for the best fitting fault parameters and found the results to be similar to the seismic solution though offset about 4 km to the northwest (Table 1). We did not fix any of the nine parameters (location, strike, dip, depth, width, length, and slip) in the first inversion. In order to estimate some errors, we fixed the location,

depth, length, and width for the final inversion. For various intermediate inversions we found that the location of the fault and the strike and dip did not vary substantially. The fault dimensions varied by a few kilometers and there was some tradeoff between slip and fault size.

Inversions of GPS data are better suited for estimating potency (S A, fault slip x fault area) rather than moment because for the latter assumptions must be made about the fault rigidity. We estimated the moment of the earthquake using the moment magnitude relation $M_w = 2/3 \log(M) - 10.7$ [*Hanks and Kanamori,* 1979] making the assumption that MI, $\simeq M_w$. We then estimated the rigidity of the fault using the relation $\mu = M/(SA)$. The estimated rigidity of 1.9 ± 0.2 x 10^{11} dyne/cm^2 is about 35% lower than typical crustal rigidities.

We compared this value to rigidities estimated from various depth dependent velocity models for the region (rl'able 3). We used the relations $\mu = \alpha^2$. p/3, where $\lambda = \mu$, and $\mu = \beta^2 \cdot \rho$, where α and β are the P and S wave velocities respectively and ρ is the rock density [*Lay and Wallace,* 1 995], to estimate the rigidity at various depths, The estimated average rigidities for the depth range O 5 km range from 1.5 – 2.S x 10^{11} dyne/cm^2. The estimates generally are higher to the southeast and lower to the northwest near the Ventura basin. The average over all of the models for this depth range is 2.1 ± 0.5 $\times 10^{11}$ dyne/cm^2 which is within the errors of the rigidity estimated from the geodetic model. The average over models B-E, which is more appropriate to the location of the aftershock, is 1.9 ± 0.3 $\times 10^{11}$ dyne/cm^2 for the same depth range, and is nearly identical to the geodetic estimate of rigidity.

Table 3

Discussion

This rather small aftershock was detectable with GPS only because it was so shallow. Other aftershock of similar size were deeper and were not detectable with GPS. For such a small aftershock it is important to correctly estimate the farther field offsets

in order to accurately determine tile fault dimensions. We see no direct precursor or post-seismic motion during the day of this event, but the longer time, series (Figure 2) suggest that post-Northridge aseismic motions and the aftershock responded to the same stress field. Part of the strain release occurred in the aftershock while the remainder occurred aseismically.

Proper estimates of rigidity arc important to determining accurate moments and moment rates. 'l'his is in turn important in assessing seismic hazard. Both the seismic velocity and geodetic potency estimates imply a reduced rigidity for the upper crust compared to the mid- to low-crust. The GPS results indicate that the rigidity of the fault zone that ruptured in the January 29 aftershock does not vary substantially from the rigidity of the surrounding material.

Acknowledgments. We thank Mike Watkins **and** Greg Lyzenga for comments on the manuscript, and Greg Lyzenga, Wendy Panero, and Jay Parker for valuable assistance in developing the simplex code used in the inversions. Garth Franklin, Greg Lyzenga, and Mark Smith **assisted with collection of the** GPS **data.**

References

Haase, J. S., E. Hauksson, F. Vernon, and A. Edelman, Modeling of ground motion from a 1994 Northridge aftershock using a tomographic velocity model of the Los Angeles basinBaker, K. I)., D. J. Baker, J. C. Ulwick, and A. T. Stair Jr., Infrared enhancements associated with a bright aurora] breakup, *Bull. Seismol. Soc. Am., 86,* S1 56- S167, 1996.

Hanks, T.C., and H. Kanamori, A moment magnitude scale, *J. Geophys. Res., 84,* 2348--23.50, 1979.

Hauksson, E., and J.S. Haase, Three-dimensional *Vp* and *Vp/Vs* velocity models of the Los Angeles basin and central Transverse Ranges, California, *J. Geophys. Res., 102,* 5423-5453, 1997.

Hauksson, E., L. M. Jones, K. Hutton, The 1994 Northridge earthquake sequence in California-seismological and tectonic aspects, *J. Geophys. Res., 100,* 12335 12355, 1995.

Jones, I,., K. Aki, M. Celebi, A. Donnellan, J. Hall, R. Harris, E. Hauksson, 'T'. Heaton, S. Hough, K. Hudnut, K. Hutton, M. JohnstWn, Joyner, H. Kanamori, G. Marshall, A. Michael, J. Mori, M. Murray, D. Ponti, 1'. Reasenberg, D. Schwartz, L. Seeber, A. Shakal, R. Simpson, 11. Thio, M. Todorovska, M. Trifunic, D. Wald, and M. 1,. Zobak, The magnitude 6.7 North ridge, California, earthquake of 17 January 1994Hauksson, E., L. M. Jones, K. Hutton, The 1994 Northridge earthquake sequence in California-seismological and tectonic aspects, Science *266,* 389-397, 1994.

Pujol, J., An integrate] 31) velocity inversion-joint hypocentral determination relocation analysis of events in the North ridge area, *Bull. Seismol.* Sot. *Am.,* 6'6, S138- S155, 1996.

Lay, T., and '1'. C. Wallace, *Modern Global Seismology,* 521 pp., Academic Press, San Diego, Calif., 1995.

Zumberge, J.F., M.B. Heflin, D.C. Jefferson, M.M. Watkins, and F.H. Webb, Precise point positioning for the efficient and robust analysis of GPS data from large networks, *J. Geophys. Res., 102,* **.500.5 5017,** 1997.

A. Donnellan, and F. H. Webb, Mail Stop 238-600, Jet Propulsion Laboratory, 4800 Oak Grove Drive, Pasadena, CA 91109-8099 (e-mail: andrea@cobra.jpl.nasa.gov; fhw@cobra.jpl.nasa.gov)

Received September 5, 1997

To appear in the *Geophysical Research Letters*, 1997.

Figure 1. GPS station locations (circles) with measured (arrows with ellipses) and modeled offsets (heavy arrows), and the locations of the January 17 mainshock, and January 29 and March 20, 1994 aftershocks (open stars). The geodetic location of the January 29 aftershock is marked by a solid star.

Figure 2. Time series surrounding the January 29, 1994 aftershock. Diamonds are for data collected before the aftershock and gray squares are for data collected after the aftershock. The uncertainties are scaled 1s errors. Two solutions are shown on the day of the aftershock (January 29), one each for the time period before and after the event. Note the differing scales for each component of motion.

Figure 3. Thirty second solutions for the north component of motion at the station SAFE relative to CSUN.

Table 1. Seismic [*Hauksson et al.*, 1995] and geodetic aftershock parameters

Parameter	Aftershock	Solution
Date	94/01/29	...
Time	11:20:36	...
Latitude	34.305°	34.334°
Longitude	−118.577°	−118.604°
Magnitude	5.1	...
Potency	...	$2.6 \pm 0.3 \times 10^{-3}$ km^3
Moment	5.0×10^{23} dyne·cm	...
Depth	1.59 km	7.2 km
Strike	240°	239 ± 1°
Dip	80°	86 ± 0.003°
Slip	...	74 ± 48mm
Rake	−20°	−61 ± 31°
Strike-slip	...	35 ± 37mm
Dip-slip	...	−65 ± 51111111
Length	...	5.0 km
Width	...	7.3 km
Rigidity	...	$1.9 \pm 0.2 \times 10^{11}$ dyne·cm

Table 2. Station offsets in mm used for the inversions. Errors are scaled 1 σ

Station	North	East	Up
CSUN	1.4 ± 2.8	0.6 ± 4.4	−16.3 ± 16.7

Table 2. (continued)

Station	North	East	Up
JPLM	3.8 ±2.6	−1.7± 4.2	--10. 8± 14.2
LNCH	1.8± 4.4	1.8 ±4.7	−39.1 ± 28.6
SAFE	--35.,5 ± 2.8	−8.3 ± 4.2	−39.7 ± 14.9

Table 3. Estimates of rigidity based on P (α) or S (β) wave velocities

Model	Depth km	Velocity 111/S	ρ km/m^3	μ dyne . cm	0- 5 km average
A[a]	1.0	3242.0	2669.0	2.8×10^{11}	2.8×10^{11}
	1..5	3246.4	2670.3	2.8×10^{11}	
	2.0	3250.7	2671.6	2.8 x 10^{11}	
	3.0	3259.3	2674.2	2.8 x 10"	
	4.0	3267.8	2676.7	2.9 X 10^{11}	
	5.0	3295.3	2685.0	2.9 x 10^{11}	
	6.0	3399.3	2716.2	3.1 x 10^{11}	
B[a]	1.0	3073.3	2618.3	$2 . 5 \times 10^{11}$	2.2×10^{11}
	1.5	2316.1	2419.1	1.3×10^{11}	
	2.0	2793.6	2534.3	2.0 x 10^{11}	
	3.0	2869.4	2557.1	2.1 x 10^{11}	
	4.0	3046.2	261O.2	2.4 X 10**	
	5.0	3203.1	2657.3	2.7 X 10^{11}	
	6.0	3344.8	2699.8	$3.0 \times 10^{1'}$	

Table 3. (continued)

Model	Depth km	Velocity m/s	ρ km/m^3	μ dyne . cm	0-5 km average
C[b]	0.5	1000.0	2650.0	2 . 7 x 1 0^{10}	1 . 7 x 10^{11}
	2.5	2900.0	2650.0	2.2×10^{11}	
	5.0	3100.0	2650.0	2.5 X 10^{11}	
	10.0	5450.0	2650.0	2.9 X 10^{11}	
	15.0	6000.0	2650.0	3.6 x 10^{11}	
D[c]	1.5	3100.0	2650.0	8..5 $\times 10^{10}$	1.5X 10^{11}
	5.0	4900.0	2650.0	2.1×10^{11}	
	7.5	5450.0	2650.0	2.6×10^{11}	
	10.0	6000.0	2650.0	3.2 X 10^{11}	
D[d]	1.0	4000.0	2650.0	1.4 XI O]]	2.1×10^{11}
	2.0	4500.0	2650.0	1.8×10^{11}	
	3.0	5000.0	2650.0	2.2×10^{11}	
	4.0	5250.0	2650.0	2.4 XI O]'	
	5.0	5500.0	2650.0	2.7 X 10^{11}	
	10.0	6000.0	2650.0	3.2x 10**	

[a]Model A and B from *Magistrale* [written communication] for the seismic and geodetic location of the aftershock respectively. Velocities in models A-C arc S wave velocities.

[b]From [1/(meet *al.*, 1996]. Density estimates are assumed for 11)0(1('1s (-E.

[c]From [*Pujol*, 1996]. Velocities are 1' wave velocities.

[d]From [*Hauksson and Haase*, 1 997]. Velocities are P wave velocities.

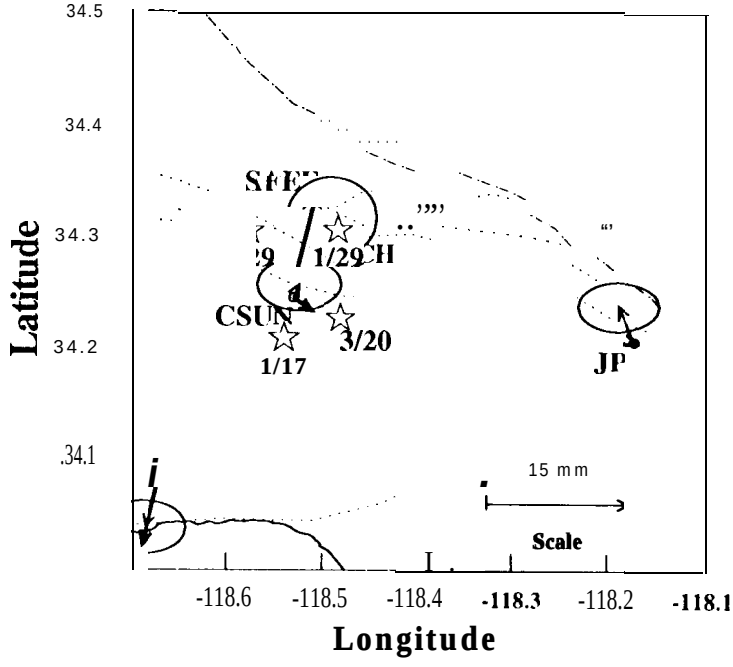
34.5
34.4
34.3
34.2
.34.1
Latitude
1/29
CSUN
1/17
3/20
JP
15 mm
Scale
-118.6
-118.5
-118.4
-118.3
-118.2
-118.1
Longitude

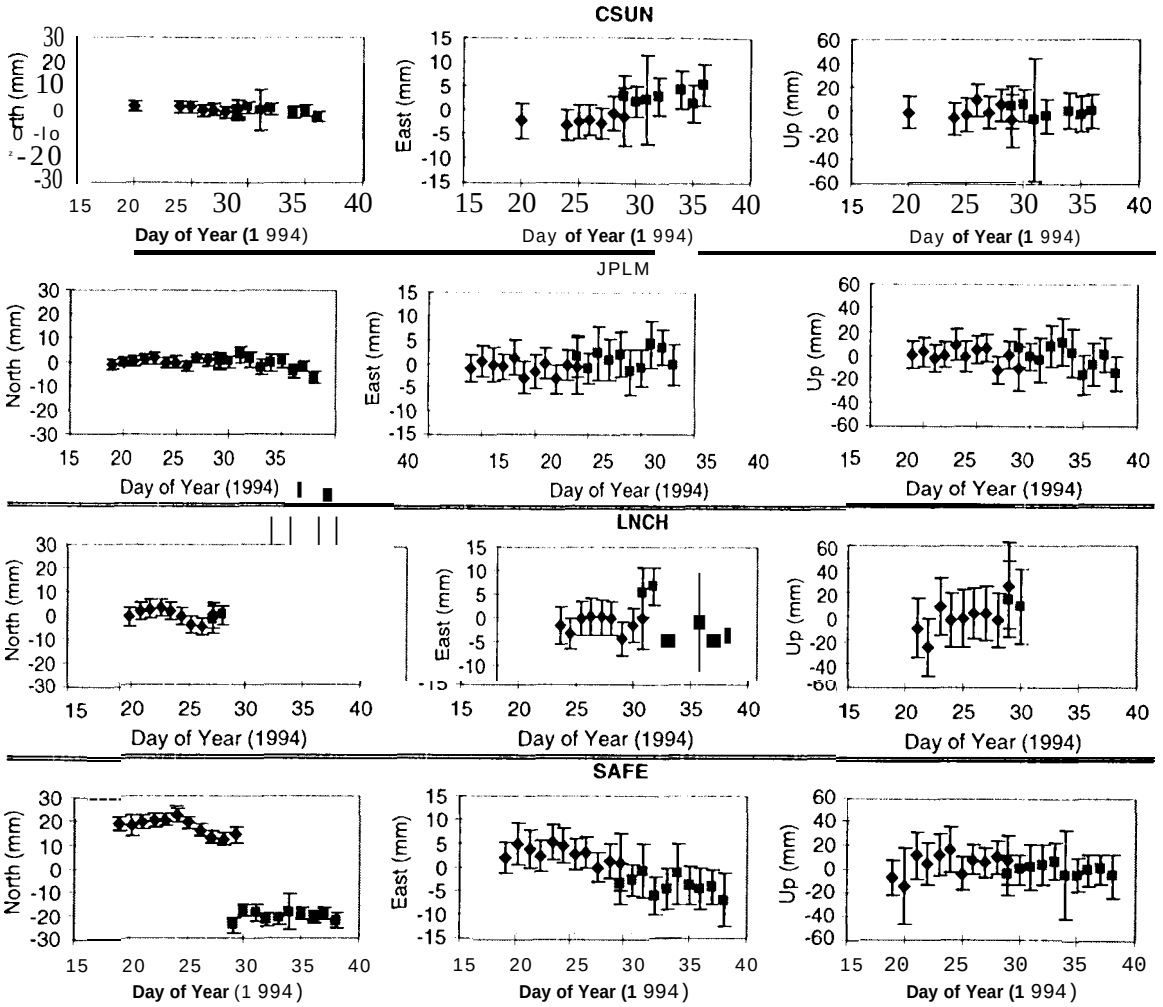
CSUN
North (mm)
East (mm)
Up (mm)
Day of Year (1994)
JPLM
LNCH
SAFE

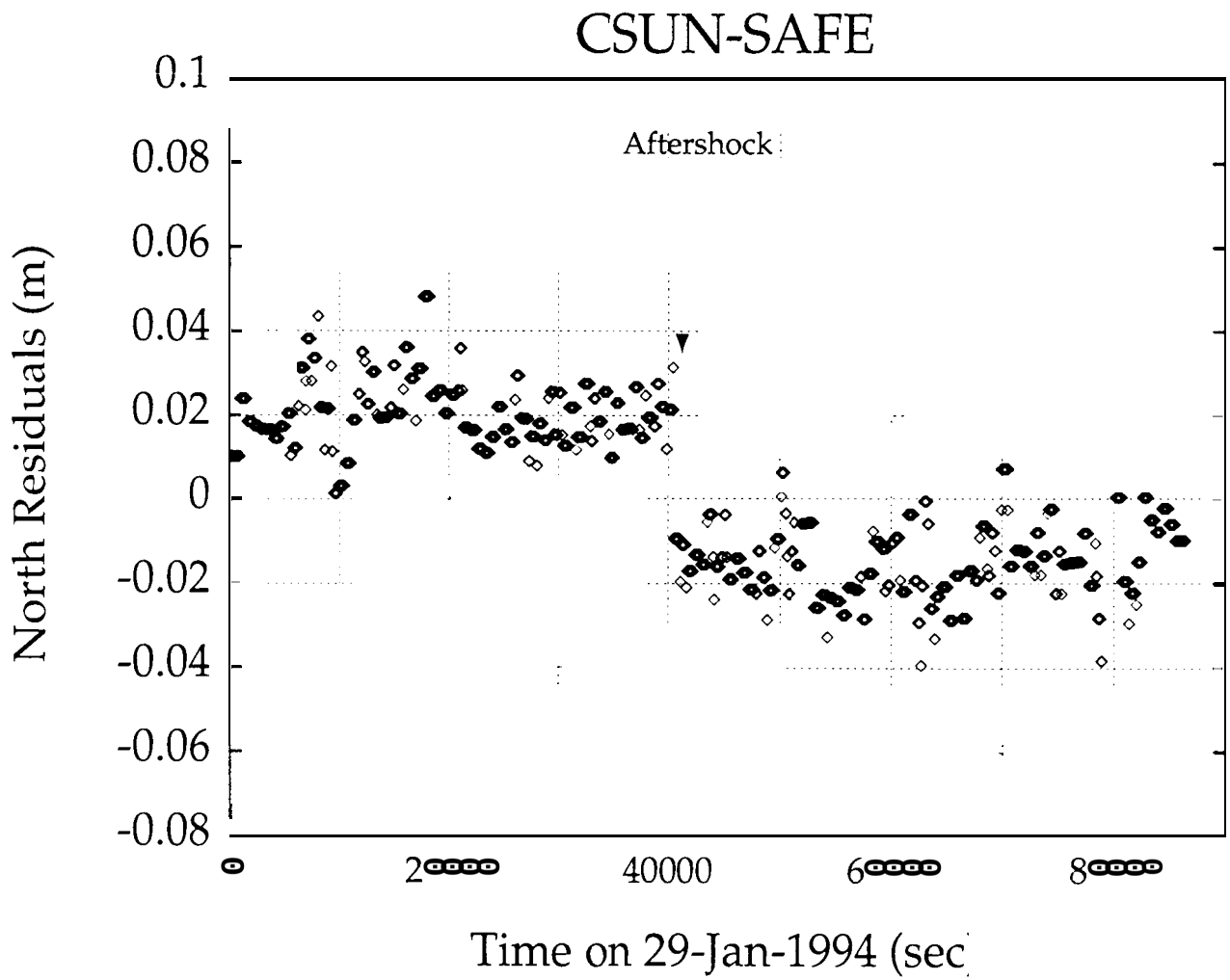
CSUN-SAFE
Aftershock
North Residuals (m)
0.1
0.08
0.06
0.04
0.02
0
-0.02
-0.04
-0.06
-0.08
0
2
40000
6
8
Time on 29-Jan-1994 (sec